Au/TiO₂ Catalyzed Benzyl Alcohol Oxidation on Morphologically Precise Anatase Nanoparticles

Akbar Mahdavi-Shakib¹, Janine Sempel¹, Maya Hoffman¹, Aisha Oza¹, Ellie Bennett², Jonathan S. Owen², Amir Rahmani Chokanlu³, Brian G. Frederick³, Rachel Narehood Austin^{1*}

- ¹ Department of Chemistry, Barnard College Columbia University, NY NY 10027
- ² Department of Chemistry, Columbia University, NY NY 10027
- ³ Department of Chemistry, University of Maine, Orono ME 04469
- * To whom correspondence should be addressed, raustin@barnard.edu or rna2113@columbia.edu

Abstract:

Au nanoparticles (NP) on TiO₂ have been shown to be effective catalysts for selective oxidation reactions using molecular oxygen. In this work, we have studied the influence of support morphology on the catalytic activity of Au/TiO₂ catalysts. Two TiO₂ anatase supports, a nanoplatelet-shaped material with predominantly the {001} facet exposed and a truncated bipyramidal-shaped nanoparticle with predominantly the {101} facet exposed, were prepared using a non-aqueous solvothermal method and characterized using DRIFTS, XPS, and TEM. Au nanoparticles were deposited on the supports using the deposition-precipitation method and particle sizes were determined using STEM. Au nanoparticles were smaller on the support with the majority of the {101} facet exposed. The resulting materials were used to catalyze the aerobic oxidation of benzyl alcohol and trifluoromethyl benzyl alcohol. Support morphology impacts the catalytic activity of Au/TiO₂; reaction rates for reactions catalyzed by the predominantly {101} material were higher. Much of the increased reactivity can be explained by the presence of smaller Au particles on the predominantly {101} material, providing more Au/TiO₂ interface area, which is where catalysis occurs. The remaining modest differences between the two catalysts are likely due to geometric effects as Hammett slopes show no evidence for electronic differences between the Au particles on the different materials.

Keywords: morphologically precise nanoparticles, titania, heterogeneous catalysts, metal-support interface, gold nanoparticles.

Introduction: Au(0) nanoparticles (NP) deposited on metal oxide supports have shown promise in green chemistry for their ability to catalyze oxidation reactions using molecular oxygen under ambient conditions with high selectivity. The metallic nanoparticle/metal oxide interface chemistry is critical for catalytic activity because oxygen does not readily dissociate on the Au surface, but is readily activated at the metal support interface (MSI).

TiO₂ is one of the most important metal oxides in heterogeneous catalysis and has been shown to be a valuable support for Au(0) nanoparticles.⁷⁻¹⁰ There are two primary crystal structures of TiO₂: rutile and anatase. Anatase is a metastable phase with nanoparticles stable at temperatures below 700 °C. It has two thermodynamically stable facets: {101} and {001}. With a lower surface energy, the {101} facet is usually the majority facet but important chemistry has been attributed to the minority {001} facet and substantial differences exist between the two.¹⁰⁻¹⁵ Understanding the role of support's exposed facet on the catalytic activity of M/TiO₂ catalysts is an active area of research.¹⁶⁻²⁰ To the best of our knowledge, the role of support morphology on the catalytic activity of Au/TiO₂ catalysts toward alcohol oxidation has not been reported previously.

Au nanoparticles on supported metal oxides have been shown to be excellent catalysts for the selective oxidation of benzyl alcohols.^{1, 21-24} In these reactions, hydride transfer from the substrate to the gold particle is the rate determining step (RDS).^{21, 22, 25}

Binding of the substrate to the support and support-assisted deprotonation of the substrate are also important steps in the overall reaction.²¹ The catalytic cycle requires O₂, which reacts with the Au(0)-supported hydride to eventually produce water and regenerate the active site.²⁶ We have recently shown that studying the oxidation of several different benzyl alcohols can provide insight into the MSI chemistry of supported metal catalysts.²¹

Saturation kinetics analysis is commonly performed in enzyme catalysis and heterogeneous catalysis to distinguish the binding/activation steps from the rate determining transformation step. A saturation kinetic analysis, which implies that the reaction rate reaches a maximum when the active site is saturated with substrate, was performed to evaluate the support morphology dependence of the activity of Au/TiO₂ catalysts for benzyl alcohol oxidation. This analysis simplifies the overall reaction by describing the reaction mechanism in two major steps, which facilitates identifying important factors that influence reaction rates. The two steps are: (1) substrate adsorption to the active sites to form an active site-substrate complex and (2) subsequent conversion of the active site-substrate complex to the product,

$$C + S \stackrel{k_1}{\rightleftharpoons} CS \stackrel{k_2}{\rightarrow} C + P$$

$$\stackrel{k_{-1}}{\downarrow} CS \stackrel{k_2}{\rightarrow} C + P \qquad (1)$$

where C, S, and P represent the active site, substrate, and the product, respectively. The reaction rate as a function of substrate concentration is

$$v = \frac{v_{max}[S]}{K_M + [S]} \tag{2}$$

where $v_{max} = k_2[C]_T$, $K_M = \frac{k_{-1} + k_2}{k_1}$. $[C]_T$ is the total number of active sites. This analysis makes clear that when the rate is determined under conditions in which the active site is

saturated with respect to substrate (v_{max}) , the rate depends only on the rate determining step and the number of active sites.

Two important quantities extracted from this analysis are the K_M and v_{max} values, as illustrated in Figure 1. A saturation kinetics analysis also provides a way to measure the catalyst's ability to activate the substrate for reaction via K_M . If $k_{-1}\gg k_2$, then $K_M\cong\frac{k_{-1}}{k_1}=\frac{1}{K_{asmb}}$, as we showed recently using kinetic isotope labeling experiments. Years is the assembly equilibrium constant and the product of all of the equilibrium constants of the steps before the rate-determining step which, in the reaction being studied here, is the transfer of a hydride. The v_{max} is the limit of the reaction rate at high substrate concentrations and is dependent on the rate constant of the RDS and the number of active intermediates at the MSI.

This analysis is performed as a Michaelis-Menten (M-M) analysis in the enzymatic literature and as a Langmuir-Hinshelwood (L-H) analysis in the heterogeneous catalysis literature. The L-H analysis is equipped with more tools to describe the adsorption of multiple substrates and the impact this has on surface coverages. However, at the level of analysis performed in this work, both approaches give identical results. We adopt the M-M terminology in this work for ease of communication.

$$K_{ads} \times K_{a} = K_{asmb} = \frac{1}{K_{M}}$$

$$V_{max} = k_{2}[Au_{active}]$$

$$MO_{x} Support$$

$$RCH_{2}OH + MOH \stackrel{K_{ads}}{\rightleftharpoons} RCH_{2}OH + MOH_{2}^{+} deprotonation$$

$$RCH_{2}OH + MOH \stackrel{K_{ads}}{\rightleftharpoons} RCH_{2}O^{-} + MOH_{2}^{+} deprotonation$$

$$RCH_{2}OH + MOH \stackrel{K_{ads}}{\rightleftharpoons} RCH_{2}O^{-} + MOH_{2}^{+} deprotonation$$

$$RCH_{2}OH + Au - H^{-} + 1/2 O_{2} \longrightarrow Au + MOH + H_{2}O \quad fast$$

Figure 1. Saturation kinetic analysis of benzyl alcohol oxidation. Adapted with permission from ACS Catalysis.²¹

Hammett parameters are a classic tool from the physical organic literature²⁷ that have been widely used to study reaction mechanisms in both homogeneous²⁸⁻³⁴ and heterogeneous reactions^{25, 35-39}. Recently, they have been developed as a powerful way to probe active site electronics in solids.^{21, 22, 40-44} In a Hammett study, reactions are done with substrates that contain a phenyl ring that has been substituted (usually in the *para* position) with substituents of varying electron-donating or electron-withdrawing abilities. The electron-donating or electron-withdrawing properties are quantified with a Hammett parameter. Reaction rates are measured and information about the electronic structure of key steps in the reaction mechanism can be determined. Since the rate-determining step for the oxidation of benzyl alcohol to the corresponding aldehyde involves the transfer of a hydride to the Au particle (as shown above in Figure 1), a reaction catalyzed

with an Au/metal oxide catalyst with a more electron-rich Au particle will have a higher energy barrier for hydride transfer and hence be less sensitive to the electronic effects of the benzyl ring substituents.²² The result will be a smaller Hammett slope for this material. A reaction catalyzed by a less electron-rich Au particle will have a lower energy barrier for hydride transfer and hence be more sensitive to the electronic effects of benzyl ring substituents and therefore have a larger Hammett slope.²²

To examine the effect of exposed facets on the catalytic activity of Au/TiO₂, we synthesized two titania nanoparticles with different morphologies. Recent advances in material synthesis have made it possible to synthesize morphologically precise anatase nanoparticles that differ dramatically in the relative ratio of the {101} to {001} facets. 11 We used these materials as supports for Au(0) catalysts and studied their reactivity towards benzyl alcohol oxidations. K_M and v_{max} values were determined for both catalysts. The K_M values were similar, showing that the interaction of the substrate with the active site was similar between the two materials. The v_{max} values were larger on the material with a greater proportion of the {101} facet, which accommodates the formation of smaller Au NP sizes, consistent with prior reports. 19 Turnover frequencies (TOF) measured in terms of moles of product per mole of Au were also larger for the material with the greatest proportion of the {101} facet, and were similar to TOF reported for other supported Au catalysts. 45-47 When TOF were defined in terms of moles of product per mole of Au in perimeter sites, which is where catalysis is thought to occur, differences between the two materials were greatly reduced. Several explanations for the observed behavior are proposed below.

Results:

The development of methodologies that facilitate the synthesis of morphologically precise metal oxide nanoparticles has generated a great deal of interest, enabling exploration of many metastable materials. 48-51 Since the discovery of methods to control the morphology of anatase TiO₂, ¹¹ significant effort has been devoted to achieve better control over the relative exposed facets and toward understanding the morphology-dependent catalytic activity of TiO₂. Gordon et al. developed a non-aqueous synthetic procedure that enables the aspect ratio of the {101} and {001} surfaces of titania (anatase) to be tuned by varying the titania precursor and the surfactant.⁵² In this paper, we synthesized the two anatase morphologies on either end of the Gordon et al. series, one with a majority {001} surface, the other with a majority {101} surface. These were then used as supports on which to deposit Au nanoparticles to form selective alcohol oxidation catalysts. We made two catalysts for this study. F-ODOL (as it is identified in this paper) was made with TiF₄ and 1-octadecanol (ODOL) as the surfactant and, under these conditions, nanoplatelets form with a majority of the {001} surface exposed. CI-ODOL (again, the identifier used in this paper), was made with TiCl₄ and ODOL, and under these conditions truncated bipyramidal nanoparticles form with a majority of the {101} surface exposed (Figure 2). Over the course of repeated syntheses, details were noted that were critical to producing reproducible catalytic materials. Specifically, we found that CI-ODOL must be washed with water instead of toluene after it is synthesized and that it is important to wash the synthesized materials with ammonium hydroxide rather than sodium hydroxide to remove fluoride ions while retaining surface hydroxyls that are important for reactivity. TEM images confirm the morphology of the two types of samples that we prepared (Figure 3).

As synthesized, the CI-ODOL sample was light yellow and the F-ODOL sample was blue. Below we present results from these materials' characterization in addition to reporting the catalytic activity of the resulting materials. Additional synthetic details are provided in the experimental section.

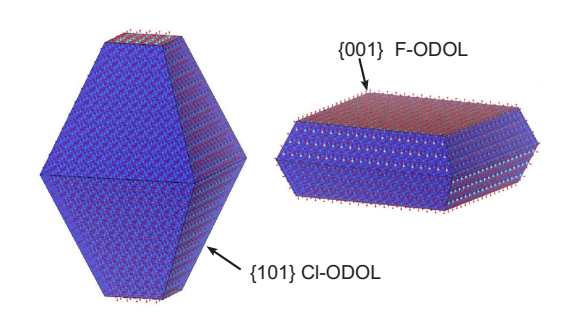


Figure 2. Representations of the different anatase morphologies used in this work.

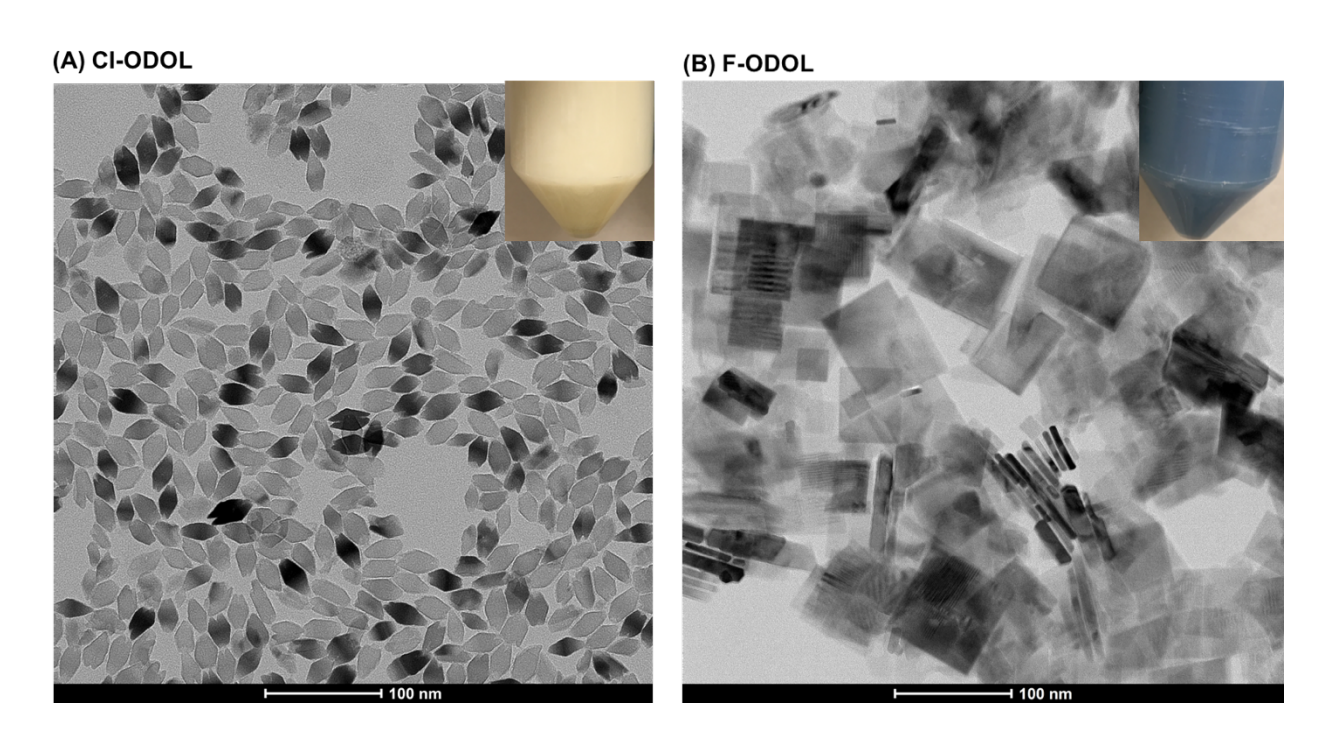


Figure 3. TEM images of the anatase TiO₂ supports (A) Cl-ODOL and (B) F-ODOL. Insets show the pictures of the as-synthesized samples dispersed in water and toluene, respectively.

Diffuse reflectance infrared Fourier transform spectroscopy (DRIFTS)

After the materials were synthesized, several work-up steps were undertaken before depositing Au nanoparticles on the surface: (1) ligand-exchange to remove surfactants, (2) a base wash to remove the halogens, and (3) calcination at 300 °C to remove organic impurities and defects. The sample was treated with NOBF4 to remove the organic capping ligands and treated with NaOH to remove residual fluoride before the DRIFTS experiments of Figure 4. Figure 4A shows the DRIFTS spectra recorded during the calcination of F-ODOL TiO₂ from 30 °C to 300 °C in dry O₂ flow. The blue color of the as synthesized F-ODOL is attributed to the presence of shallow trap states.⁵² The DRIFTS spectrum recorded at 30 °C shows a broad background absorbance stretching from 7000 cm⁻¹, the upper limit of our instrument, to 1000 cm⁻¹, where phonon modes start to absorb light. This broad electronic absorbance (BEA) in the IR region is attributed to the absorption of IR light by shallow trap and conduction band electrons. 53-55 Heating the sample to 200 °C under O₂ did not significantly change the BEA or the blue color of the sample, indicating that the defects associated with these trap states are very stable. When the temperature was increased to 300 °C, both the BEA of the DRIFTS spectra and the blue color of the sample slowly disappeared. Figure 4B shows the difference spectrum between 300 °C and 30 °C, which can be assigned to contributions from shallow trap electrons and conduction band electrons. 53-55 The decrease in the BEA upon calcination at 300 °C, accompanied by the observed color change, indicates that both shallow trap and conduction band electrons were eliminated (oxidized) upon calcination at 300 °C. The color of the sample remained light taupe when the temperature was reduced to 30 °C.

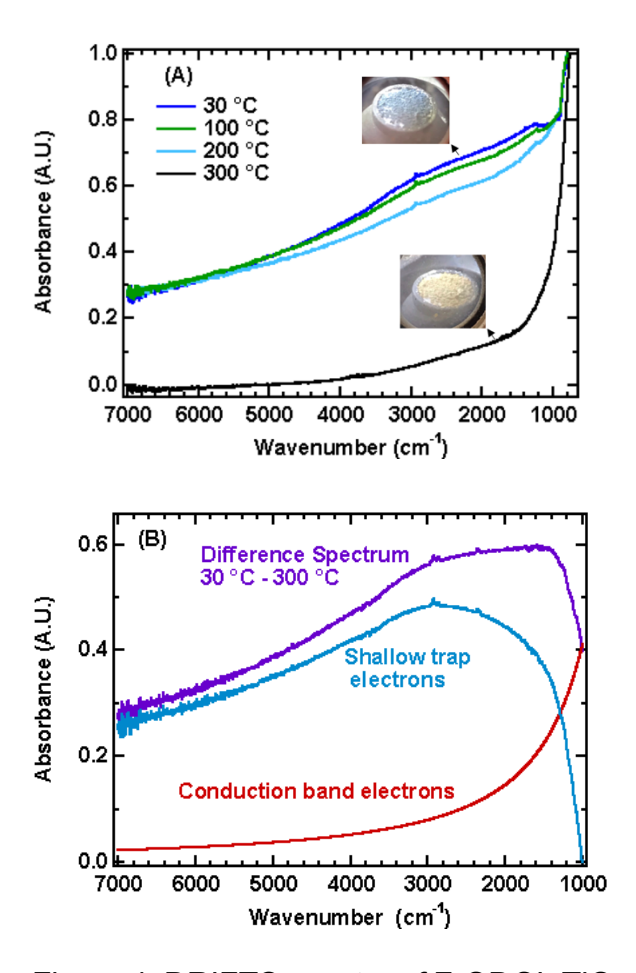


Figure 4. DRIFTS spectra of F-ODOL TiO₂ (after ligand exchange and NaOH wash) using *in-situ* calcination in the DRIFTS chamber. (A) DRIFTS spectra recorded during the calcination from 30 °C to 300 °C. The sample was kept at each temperature at least for 1 hour. Spectra were referenced to the single beam of KBr. (B) Difference DRIFTS spectrum obtained by subtracting the 300 °C spectrum from the 30 °C spectrum. The red line is the IR absorbance by the conduction band electrons as described by the $Abs = A\tilde{v}^{-1.5}$. The blue line which is attributed to the IR light absorbance by shallow trap electrons⁵³ and was obtained by subtracting the red line from the purple spectrum.

Surface hydroxyl bands (3600-3800 cm⁻¹) were not observed for the sample washed with NaOH, Figure 4. This could be because Na⁺ ions can exchange with the surface hydroxyl protons (Ti-OH + Na⁺ \rightarrow Ti-ONa + H⁺).⁵⁷ To preserve the surface hydroxyls, we therefore used NH₄OH as the base for fluorine removal in subsequent experiments.

Figure 5 shows the DRIFTS spectra of CI-ODOL after ligand exchange and NH₄OH wash, recorded during the calcination in the DRIFTS cell. This sample was yellow as synthesized, not blue in contrast to F-ODOL, indicating that it does not have the same defect-associated trap states. The BEA was not observed in the DRIFTS spectrum of this sample, consistent with the absence of shallow traps and conduction band electrons. The spectrum of the CI-ODOL sample recorded at 50 °C contains bands in the 1200-1600 cm⁻¹ range that could be from carbonates and/or hydrocarbons, the water bending band at 1620 cm⁻¹, aliphatic C-H stretching bands at 2800-3000 cm⁻¹, O-H stretching bands of H-bonded surface hydroxyls and H-bonded water molecules at 2500-3600 cm⁻¹, and O-H stretching of the isolated surface hydroxyls at 3600-3750 cm⁻¹. After calcination of the sample at 300 °C, only carbonate bands in the 1200-1500 cm⁻¹ range and isolated O-H bands at 3600-3750 cm⁻¹ remained. These species are commonly present on TiO₂ surfaces. Similar features were observed in the DRIFTS spectrum of the F-ODOL sample after a similar work-up procedure (Supporting information, Figure S1).

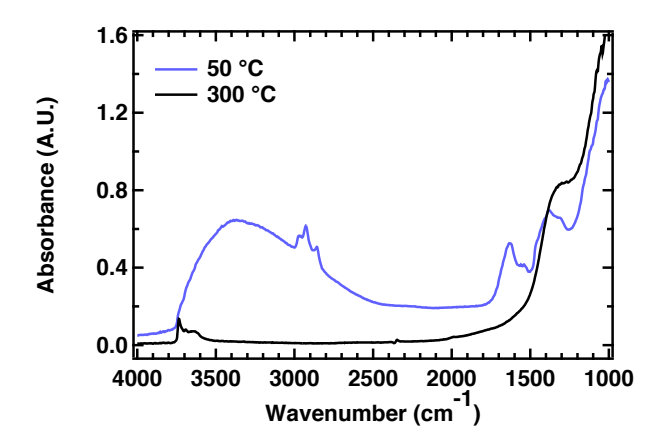


Figure 5. DRIFTS spectra of CI-ODOL (ligand-exchanged and washed with NH₄OH) recorded during the calcination in a dry oxygen stream. The sample was heated at each temperature overnight. For clarity, only the 50 °C and 300 °C spectra are plotted.

X-ray photoelectron spectroscopy (XPS)

When evaluating morphology-controlled materials as potential supports for noble metal catalysts, there are two questions that need to be addressed: (1) are the structure-directing capping agents removed after work-up? and (2) is the morphology retained after work-up?⁵⁸ These questions are important because surface hydroxyls, which would be liberated after the structure-directing capping agents are removed, are used in the catalytic reaction and because it is meaningless to compare the effects of particle morphology if the particle morphology is not retained during work-up. We have addressed these two questions in this section.

Figure 6A shows XPS analysis of the F-ODOL sample. The as-synthesized F-ODOL TiO₂ calcined at 300 °C showed a F(1s) peak at 685 eV indicating that calcination at 300 °C is not sufficient for fluorine removal. No efforts were made to calcine the sample at higher temperatures because the {001} surface is known to undergo reconstruction at higher temperatures and, as a result, lose surface hydroxyls.^{59, 60} After ligand exchange, treatment with NH₄OH and then calcination at 300 °C, the F(1s) peak was largely eliminated. However, a very small peak at 686.5 eV remained. This peak was assigned to a two-coordinated (bridging) fluorine species, identified by Sheng *et al.*⁶¹ These difficult to remove fluorines could impact the electronic structure⁶² and surface acid/base properties of this material⁶³. TEM analysis of the sample after such treatment shows that morphology is retained, Figure 6B.

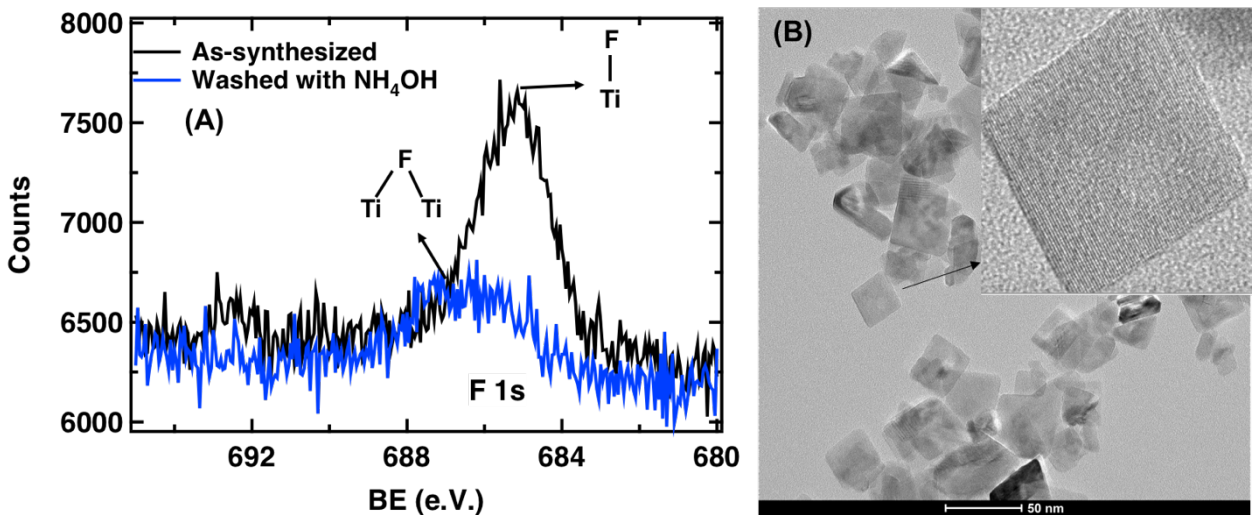


Figure 6. XPS spectra of the as-synthesized sample calcined at 300 °C (black spectrum) and the sample calcined at 300 °C after ligand-exchange and pretreatment with a 30% NH₄OH solution (blue spectrum). (B) TEM image of the F-ODOL sample calcined at 300 °C after ligand-exchange and pretreatment with a 30% NH₄OH solution, showing that the morphology is retained.

Figure 7 shows the XPS spectra of CI-ODOL in the CI(2p), N(1s), and F(1s) regions at different stages of work-up. The as-synthesized sample showed CI(2p), but not N(1s) or F(1s) peaks. After the ligand-exchange step, the CI(2p) peak was eliminated while N(1s) and F(1s) peaks appeared in the XPS spectra, probably coming from acetonitrile and NOBF₄ which are used in the ligand exchange step. After stirring the sample in a concentrated (2s-30%) NH₄OH solution and then drying overnight at 120 °C, chlorine, fluorine, and nitrogen impurities were below the detection limit of XPS. The material's morphology was retained (Figure 7D).

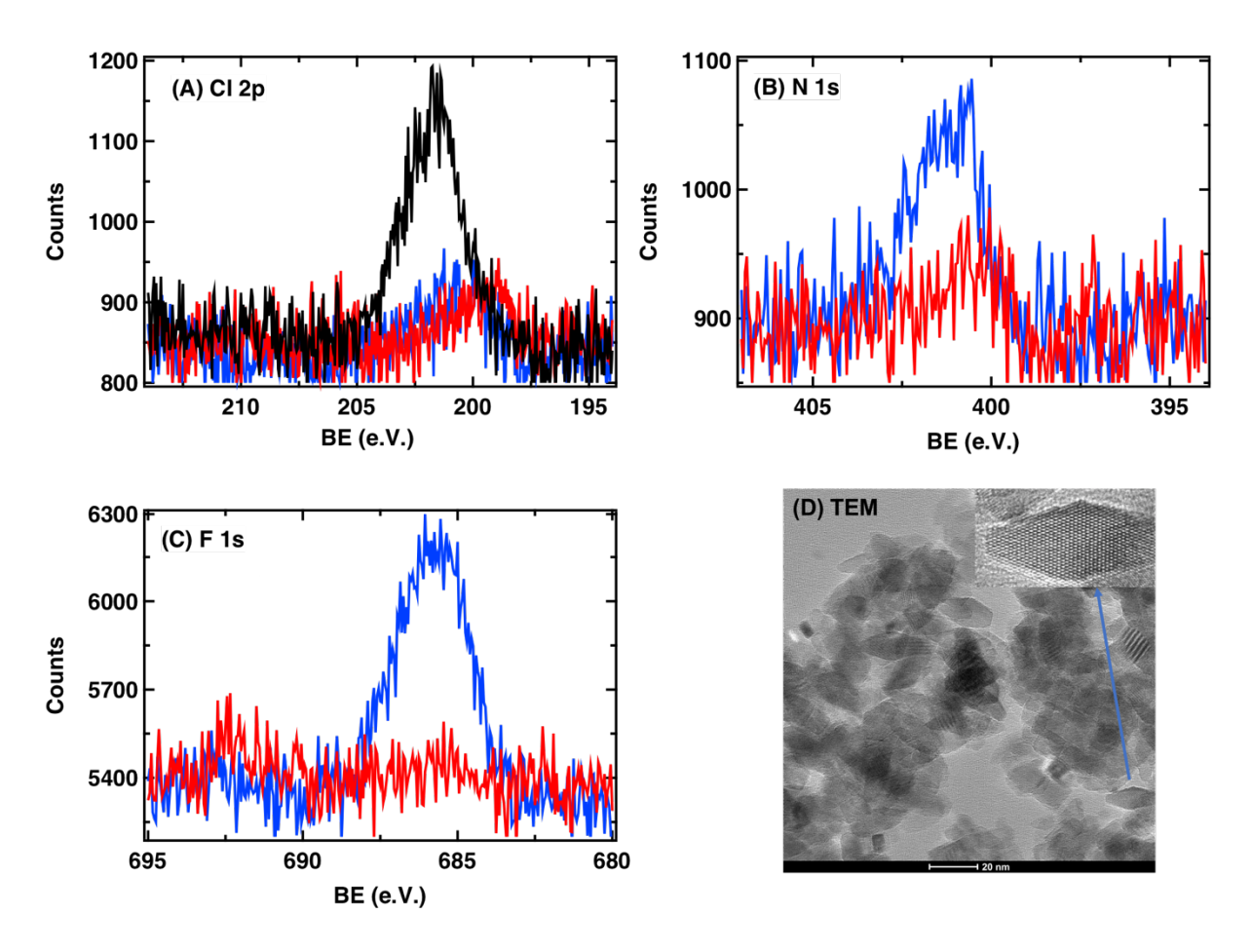


Figure 7. XPS spectra of anatase CI-ODOL in (A) CI 2p, (B) N 1s, and (C) F 1s region. As-synthesized (black), after ligand exchange reaction using NOBF₄ in acetonitrile (blue), and after base treatment using NH₄OH (red). (D) TEM image of the CI-ODOL sample after work-up procedure, showing that after ligand exchange, base wash with concentrated NH₄OH, and calcination at 300 $^{\circ}$ C the morphology is retained.

Deposition and characterization of Au nanoparticles

Au nanoparticles were deposited on the treated anatase samples using the deposition-precipitation method^{64, 65} (as described in the experimental section) and reduced with H₂ at 200 °C. Figure 8 shows the particle size analysis done from STEM images by measuring at least 200 Au nanoparticle sizes (one representative image is

shown in the inset). The average Au particle size on F-ODOL support was 3.5 (± 1) nm and on the CI-ODOL support it was 2.0 (± 0.7) nm.

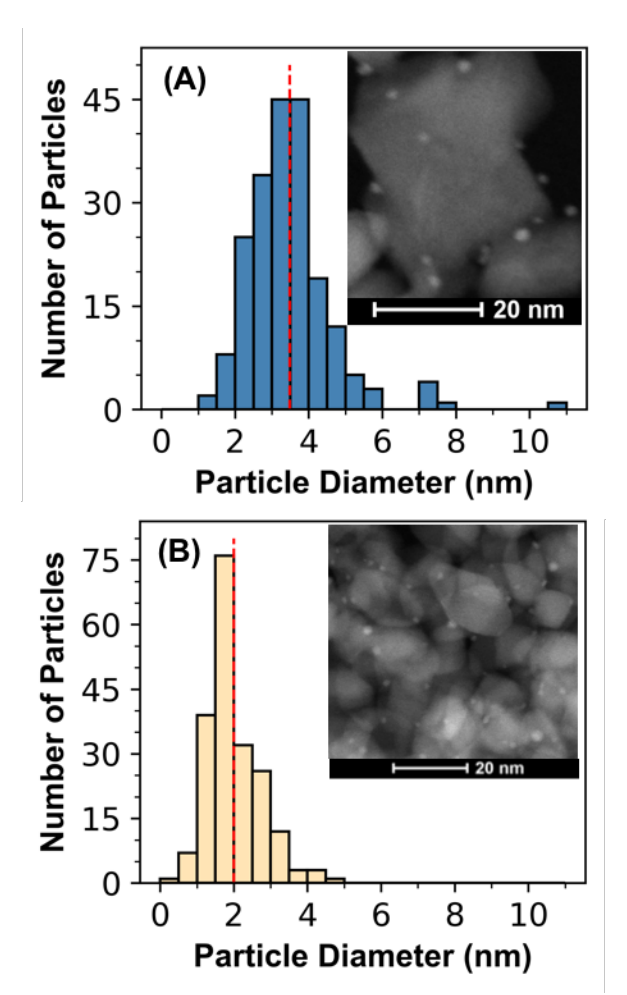


Figure 8. Au particle size distribution of (A) Au/F-ODOL and (B) Au/Cl-ODOL. The average Au nanoparticle size was $3.5 (\pm 1)$ nm and $2.0 (\pm 0.7)$ nm respectively, shown as dashed vertical lines. A representative STEM image is shown in the inset and full STEM images are shown in the supporting information, Figures S2 and S3.

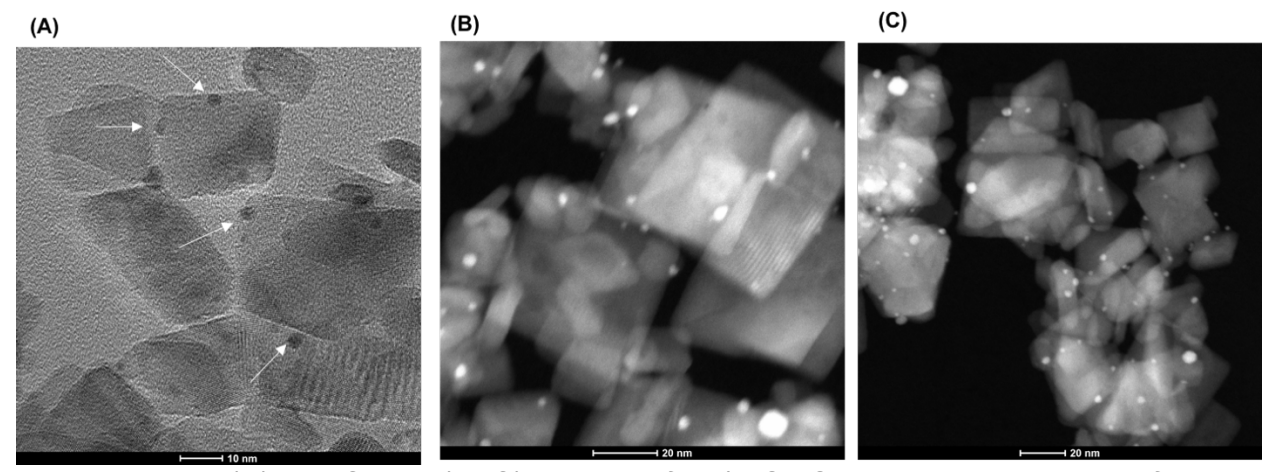


Figure 9. TEM (A) and STEM (B, C) images of Au/F-ODOL catalyst showing preferential growth of Au NPs (white particles) on the edges of nanoplatelets.

Figure 9 shows that Au nanoparticles are preferentially formed on the edges of nanoplatelets, as shown by arrows in panel A. Although it is difficult to unambiguously determine this using the TEM and STEM images because some TiO₂ particles are stacked on top of each other, it is clear that the majority of the Au nanoparticles are formed on the edges of the nanoplatelet anatase particles. This shows that Au nanoparticles are either formed on the minority {101} surfaces or at the interface of {101} and {001} surfaces. Pt nanoparticles have been found to preferentially form on {101} surfaces, especially when those surfaces are terraced.⁶⁶⁻⁶⁹

Catalytic reactivity:

Both Au/F-ODOL and Au/Cl-ODOL were used to catalyze the mechanistically well studied oxidation of benzyl alcohol and trifluoromethyl benzyl alcohol (F₃C-BA).^{22, 25, 70} Benzyl alcohol binds to the catalyst surface and is deprotonated in a series of rapid steps.²¹ The RDS is the transfer of a hydride from the substrate to the Au nanoparticle.^{21, 22}

Benzyl alcohol oxidation was performed at 60 °C using toluene as the solvent with O₂ continuously passing through the head space of the reaction vessel. The reaction solution was sampled at different time intervals and analyzed using GC-MS to measure

the rates. Oxygen limitation can slow the reaction rate.²¹ We observed that keeping O_2 out of the system by purging the reaction vessel with Ar drastically reduced the reaction rates; however, having air or pure O_2 in the headspace did not impact the reaction rates.²¹ This indicates that benzyl alcohol oxidation is O^{th} order in O_2 under our conditions. In addition, we have shown that reaction rates are not impacted by increasing the stirring rate and scaled with respect to the catalyst mass.²¹ These observations in addition to the observation of catalyst saturation under our conditions showed that the measured rates are not limited by the internal and external mass transfer rates. The reported rates are initial rates. There is a 20% uncertainty in the measured reaction rates under these conditions. Conversion versus time plots, obtained from the areas of GC-MS peak, are shown in the SI (Figures S4-S7).

Au/F-ODOL and Au/Cl-ODOL catalysts are both highly selective catalysts for the oxidation of benzyl alcohols, generating the aldehyde as the only detectable product in all cases. Figure 10 shows the saturation plots of F_3C -BA and BA oxidation. The rates for both catalysts increased with substrate concentration and reached a maximum value, indicating catalyst saturation. Double reciprocal plots were used to extract K_M and V_{max} values for each substrate-catalyst system (Figure S8). The extracted values are provided in Table 1.

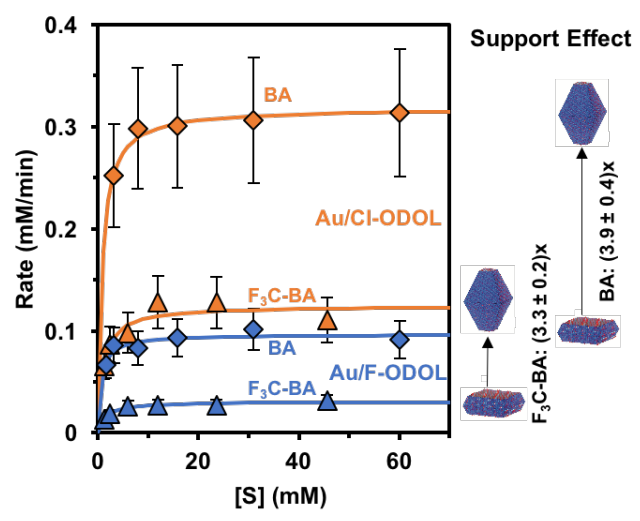


Figure 10. Saturation kinetics analysis of F₃C-BA and BA oxidation over Au/F-ODOL and Au/Cl-ODOL catalysts, plotting the dependence of the initial rate on substrate concentration under conditions of constant catalyst mass. The symbols are the measured rates and the lines are made from $\nu = \frac{\nu_{max}[S]}{K_M + [S]}$ equation, using the extracted values from double reciprocal plots, shown in the supporting information. The extracted values are summarized in Table 1, showing that there is a significant increase in ν_{max} for both substrates on Au/Cl-ODOL compared to Au/F-ODOL, which is also illustrated in the image in the right-hand margin of the figure.

Table 1. Comparison of the two catalysts for F₃C-BA and BA oxidation at 60°C.

Substrate	Catalyst	K _M (mM)	V _{max}	^a TOF per mole	bTOF per mole of Au
			(mM/min)	of Au	in perimeter sites
				(min ⁻¹)	(min ⁻¹)
F ₃ C-BA	Au/CI-ODOL	1.1 ± 0.2	0.12 ± 0.01	0.5 ± 0.05	4.5 ± 1.0
	Au/F-ODOL	1.5 ± 0.1	0.031 ± 0.001	0.1 ± 0.01	2.4 ± 0.6
BA	Au/CI-ODOL	0.8 ± 0.1	0.318 ± 0.005	1.5 ± 0.2	12.0 ± 2.5
	Au/F-ODOL	0.7 ± 0.2	0.097 ± 0.004	0.4 ± 0.04	7.6 ± 1.7

^a Defined as moles of product per mole of Au per minute and considering 10% uncertainty in the measured catalyst mass and 0.02 mL uncertainty in the measured volumes. ^b Normalized per number of perimeter Au atoms. Details are shown in the supporting information. Uncertainties are measured using regression analysis of the double reciprocal plots (for the v_{max} and K_M values) shown in the supporting information, and considering 10% uncertainty in the measured catalyst mass, 0.02 mL uncertainty in the measured volumes, and 10% uncertainty in the perimeter length.

The maximum rate (v_{max}) for the oxidation of F₃C-BA and BA were respectively 3.9 \pm 0.4 times higher and 3.3 \pm 0.2 times higher for the Au/Cl-ODOL catalyst compared to Au/F-ODOL. These rates were determined using identical amounts of catalysts, both

having a similar amount of gold. Thus, per gram of catalyst, the Au/Cl-ODOL material is a better catalyst.

Different measures of "catalytic goodness" are used in the literature. TOF are often reported but even these can be defined in different ways. If defined as moles of product per mole of Au atoms per unit time (minute), these catalysts all have TOF between $2.0 - 0.1 \frac{mole\ of\ product}{mole\ of\ Au*min}$, which is comparable to other published results (Table 1).⁴⁵⁻⁴⁷ By this measure, the Au/Cl-ODOL catalyst was approximately 5 times better than the Au/F-ODOL catalyst.

It is also useful to evaluate the two catalysts in terms of the activity per active sites. While the exact nature of the active site is not clear, it is likely to be at the perimeter between the Au particles and the metal oxide surface. $^{21, 22, 71, 72, 73, 74}$ When the TOF is calculated using an estimate of the number of Au atoms at the metal support interface differences between the two materials diminish. By this measure, the Au/Cl-ODOL catalyst is about 1.5 times better than the Au/F-ODOL material. Notably, the TOF for the Au/Cl-ODOL catalyzed oxidization of benzyl alcohol reported in this way (12.0 \pm 2.5) is in excellent agreement with the TOF previously reported in the same way for Au/TiO₂ from Strem Chemicals, which uses P25 as the titania support (13 \pm 2). 74 (More information on this analysis can be found in the supporting material.)

The oxidation of benzyl alcohol was faster than the oxidation of F_3C -BA for both catalysts. The trifluoromethyl group is strongly electron-withdrawing, destabilizing the cationic intermediate on the substrate, and slowing the rate of the reaction, consistent with the Hammett relationship reported for the oxidation of benzyl alcohol over other supported Au catalysts.²¹⁻²³ A Hammett analysis comparing the two catalytic materials

shows no difference in the Hammett slopes for these two materials, within the uncertainty of the measurements. The measured Hammett slope for the Au/Cl-ODOL and Au/F-ODOL catalysts were -0.73 ± 0.07 and -0.85 ± 0.05 respectively. (Described in more detail in the supporting material, see Eq S.5.)

K_M is independent of the number of active sites and depends on the equilibrium constants for substrate binding and deprotonation. Recently, we showed that K_M decreases as the electron-richness of the alcohol increases because more basic alcohols bind more strongly to the catalyst surface.²¹ When comparing the same substrate, differences in K_M reflect differences in the ability of the catalysts to deprotonate and bind the substrate. Our results showed no appreciable difference in the measured K_M values between Au/Cl-ODOL and Au/F-ODOL catalysts.

Discussion

This work reports the synthesis of Au nanoparticles on morphologically precise anatase titania to explore whether the surface facets of TiO₂ have a measurable impact on the reactivity of Au/TiO₂ catalysts. This work was spurred by curiosity over whether the minority surface in the anatase component of the commonly used pyrogenic titania (P25 and P90) might play an outsized role in catalysis. P90 and P25 are made of discrete anatase and rutile nanoparticles, with P90 having slightly more anatase (87.5% v. 84.6%) than P25.⁷⁵ As we recently demonstrated using atomic pair distribution analysis, the anatase fraction of P90 is best fit to a truncated bypyramid with ~20% {001} faceting and 80% {101} faceting.⁷⁵ How much of the reactivity associated with noble metal catalysts supported on titania could be explained by the minority {001} surface? To study this

question, two anatase TiO₂ materials with highly different ratios of the {101} and {001} surfaces were prepared using the same synthetic method, varying only the source of titanium, TiCl₄ or TiF₄. Fluoride ions reduce the surface energy of the anatase {001} surface compared to the anatase {101} surface.¹¹ Therefore, material prepared in the presence of fluoride ions contains primarily the {001} facet, forming particles with nanoplatelet morphology. Material prepared using TiCl₄ contains primarily the {101} facets and form nanocrystals with truncated bipyramid morphology.⁵² Both assignments were confirmed by TEM analysis.

Repeated syntheses revealed consistent color differences, with F-ODOL being blue and Cl-ODOL yellow. DRIFTS characterization of the support showed that the blue color of the F-ODOL material is due to the presence of stable shallow trap states in this material. Although the blue color of the F-ODOL was removed after calcination at 300 °C, it appeared again after deposition of Au nanoparticles. A light blue color was visible in the undissolved support after Au was dissolved using aqua regia, indicating that some of the defect states creating the blue color were generated again during catalysts preparation, probably during the reduction of the catalysts with H₂ at 200 °C. The persistence of these shallow trap states under the strongly oxidizing condition of aqua regia is surprising, but is consistent with our DRIFTS characterization results that indicate that such states resist oxidation under pure oxygen at 200 °C. Because these color centers resist oxidation, we conclude that they are not accessible to surface treatments and therefore unlikely to impact reactivity.

The biggest impact that the support morphology had on Au/TiO₂ catalysts was in the size of the Au particles they supported. Consistent with prior published work by Li *et*

al., Au nanoparticles were larger on F-ODOL, the support where the {001} surface made up the majority of the exposed surface area. Li et al. attribute the morphological dependence of Au particle size to the presence of defects, which they measured and quantified using electron paramagnetic resonance (EPR) spectroscopy. Au nanoparticles nucleate at defect sites and so the {001} surface, which possesses fewer defects, supports fewer nucleation events, and subsequently grows larger Au nanoparticles. A deeper understanding of the chemistry behind such behavior requires DFT calculations of the morphology- dependent electronic structure/defect density of anatase nanoparticles as well as adsorption energy of Au nanoparticles on the (001) surface, (101) surface, and the interface between these two surfaces.

The measured (v_{max}) values were larger for the Au/Cl-ODOL catalyst. TOF when defined in terms of moles of product per mole of Au atom per unit time were also larger for the Au/Cl-ODOL catalyst (4-5 times larger for Au/Cl-ODOL than Au/F-ODOL) and were comparable to other supported Au catalysts reported in the literature⁴⁵⁻⁴⁷, showing no catalytic benefit to using these morphologically precise materials. The benefit of these materials lies in their potential to shed light on mechanistic questions in heterogeneous catalysis. When TOF were defined in terms of moles of product per mole of active Au, i.e. Au atoms at the MSI, the difference between these two materials was greatly diminished, pointing to the importance of the interface in these reactions. A modest difference in reactivity (about 1.5 larger for Au/Cl-ODOL than Au/F-ODOL) between the two catalysts remained. Similarity between the Hammett slopes for these two materials indicate that the differences cannot be ascribed to differences in the electronic structure of the Au particles.²² The existence and source of particle size effects in supported Au catalysts,

and supported noble metal catalysts more generally, are widely debated. They are often divided into electronic and geometric effects.⁷⁶⁻⁷⁸ In the absence of evidence for electronic effects, we ascribe the remaining differences between these two catalysts to unique structural features of the MSI.^{76, 79-81}

The F-ODOL sample contains more residual fluorine (3% of the total sample is F as opposed to 0.5% with Cl-ODOL) that might impact its electronic structure. 82,83 Fluoride ions create filled shallow trap states 62 that may donate electrons to the Au nanoparticles and could mask what would otherwise be an enhanced activity of Au nanoparticles on the anatase {001} surface in the absence of fluorine. Although this is possible, it is hard to disentangle these two effects from each other because residual fluoride ions (especially in the bridging form) are difficult to remove from TiO₂ surfaces without surface reconstructions. 59 Future studies are required to study the influence of added fluoride and fluoride concentration on the K_M and TOFs of benzyl alcohol oxidation over Au/TiO₂ catalysts and to more deeply probe the electronic structure of the Au particles on both supports.

Conclusion

In conclusion, we show that it is possible to synthesize Au/TiO₂ catalysts on morphologically precise anatase nanoparticles and to use these materials to catalyze the selective oxidation of benzyl alcohols. Metal oxide particle morphology can impact the properties and reactivity of heterogeneous catalysts that they support. Au nanoparticles were smaller on the anatase nanoparticles where the {101} surface predominates (Cl-ODOL). Reaction rates for the oxidation of benzyl alcohols were also faster on the Cl-

ODOL catalyst. A saturation kinetic analysis enabled the extraction of the Michaelis-Menten parameters K_M and v_{max} , which allows us to distinguish substrate binding events from the rate determining hydride abstraction step. The values for K_M , were similar between the two catalysts (CI-ODOL and F-ODOL), showing minor or no difference between the catalysts in their effects on substrate deprotonation and binding. When the TOF were defined in terms of moles of Au at the metal-support interface, the TOFs were only slightly higher for the CI-ODOL catalyst, which again affirms the importance of the Au/metal oxide interfacial perimeter to catalysis. The TOF for the morphologically presence materials indicate that the $\{001\}$ surface, which is the minority surface in anatase nanoparticles (including those found in the pyrogenic titania P25 and P90), does not play a significant role in the catalytic activity of Au/TiO₂ catalysts supported on them, at least not for the low temperature conversion of benzyl alcohols to their corresponding aldehydes.

Experimental Information:

Materials

Benzyl alcohol (99.8%), 4-methoxylbenzyl alcohol (98%), 4-(trifluoromethyl)benzyl alcohol (98%), 1,2, 4-trichlorobenzene (>99%), HAuCl₄•3H₂O (99.7%), NaBH₄ (98%), NOBF₄, AgNO₃ (99%), 1-octadecanol (99%), titanium(IV) fluoride, titanium(IV) chloride (99.9%) and oleic acid (99%) were purchased from Sigma-Aldrich. Toluene (99.9%), methylene chloride (>99.2%), and NH₄OH (29.3%) were purchased from Fisher Scientific and used as received without further purification. 1-octadecene (90%) was obtained from Sigma-Aldrich, stirred with calcium hydride overnight, and distilled prior to use. O₂ gas (Airgas) was 2.0 grade. H₂ and N₂ (Praxair) were 5.0 grade. All these gases were used

without additional purification. All H_2O was purified to a resistivity of 18.2 $M\Omega$ -cm with an Elga PURELAB Ultra purification system.

Materials synthesis.

Stock solution: Syntheses were performed following a procedure previously reported by Gordon *et al.*⁵² The synthesis scale was tripled to obtain larger quantities of material, required to synthesize sufficient catalyst for the reported experiments, while keeping the concentrations and stoichiometries the same. Because of the importance of reproducible and high-quality material for the catalytic experiments, additional detail on the synthetic procedure is provided. We note a recent report, which highlights polymerization of the solvent (1-octadecene) during this synthesis. However, as the ligands and organic materials are removed in subsequent steps, this finding will not affect the later reactions in this procedure.⁸⁵ Briefly, inside a glovebox kept in an N₂ atmosphere a stock solution of 0.2 M TiF₄ (or TiCl₄) and 1.0 M oleic acid in 1-octadecene was prepared in a Schlenk flask. The Schlenk flask was capped and transferred to a Schlenk line to be kept in an inert gas (Ar) environment. TiF₄ stock solution was heated at 80 °C for one hour to dissolve the solid TiF₄.

Synthesis: The surfactant solution was prepared in a 500 mL round bottom flask by mixing 1-octadecanol (24.3 g, 90 mmol), 1-octadecene (30.6 mL), and oleic acid (1.5 mL, 4.7 mmol). After mixing, the sample was degassed at 120 °C for one hour and then kept under an Ar atmosphere for the rest of the reaction. The temperature was reduced to 60 °C and 4.5 mL of the stock solution was added dropwise. The temperature was rapidly increased to 290 °C. Once the temperature reached 230 °C, white colloids formed. The

solution color changed to blue at 280 °C. After 10 min of heating at 290 °C, 24 mL of stock solution was added at a flow rate of 0.9 mL/min. When the addition finished, the heating mantle was removed, and the sample was allowed to cool down to room temperature.

Removal of excess surfactant:

F-ODOL: Once at room temperature, 1-ODOL crystallizes. Therefore, after the synthesis, toluene was added to dissolve 1-ODOL and the sample was transferred to centrifuge tubes. The blue TiO₂ nanocrystals precipitated out of a yellow solution after centrifugation at 5000 x g for 10 min. The yellow solution was discarded, and 30 mL toluene was added to the blue precipitate and centrifuged again. After three cycles, the solution after centrifugation was colorless. The sample was washed at least five times by repeated addition of 30 mL toluene, followed by centrifugation.

CI-ODOL: After synthesis, the color of this sample was light brown. This sample was washed with 30 mL of toluene several times as well. However, the sample clumped together, generating a substance with a gummy consistency. When water was accidentally added to this sample, the sample totally dispersed in water and formed a stable suspension that did not precipitate, even after a 10 min centrifuge at 5000 x g. The stable suspension in water was transferred to an oven at 110 °C to evaporate the water and collect the nanoparticles.

Ligand exchange: Ligand exchange to remove bound surfactant was done using NOBF₄ in acetonitrile. After removal of excess surfactants, as described above, the samples were dried in an oven at 110 °C. At this point, samples from three separate synthesis batches were combined (for a total of 1.5 g of the material). 100 mL of hexane was added to the 1.5 g of sample and mixed using ultrasonic agitation. Simultaneously, in four different 50

mL Falcon tubes, NOBF₄ (250 mg) was dissolved in acetonitrile (25 mL) by ultrasonic agitation for 30 min. All four yellow NOBF₄ solutions were added to the TiO₂ suspension in hexane and the mixture was stirred at room temperature for 30 min. The mixture was centrifuged to separate the blue precipitate from the solution.

After ligand exchange, a stable suspension is made by adding 15 mL DMF to the precipitate, without the need for ultra-sonication. This suspension was so stable that solids did not separate after 10 min centrifuging at 5000 x g. The solid can be separated from DMF only when sufficiently non-polar solvents such as hexane or toluene are added to the mixture. This strategy was used to remove impurities from the sample. The ligand-exchanged sample was suspended in 15 mL of DMF and precipitated again by addition of 15 mL of a 50/50 solution of toluene and hexane and centrifuging. This process was repeated three times. We obtained 1.26 g of F-ODOL at this stage. Impurities remained in the DMF layer.

Base wash: Washing the sample with a basic solution was used to remove halogens, fluorine and chlorine. Initially NaOH was used as the base. However, since DRIFTS spectra of the sample after washing with NaOH showed the absence of surface hydroxyls, which can occur with sodium complexation, 2.26 M NH₄OH solution was used. Under those conditions, surface hydroxyls were apparent. For the catalyst preparation, 40 mL of 2.26 mM NH₄OH solution was added to the ligand-exchange powders and samples were mixed in dark for 24 h.

Deposition of Au nanoparticles

Au nanoparticles were synthesized in a foil-wrapped flask via urea deposition-precipitation.^{86, 87} HAuCl₄•3H₂O (3 mM) and urea (0.42 M) was added to 20 mL H₂O with

stirring to target a 1-1.5% Au mass loading. This yellow/orange solution was heated with stirring until the temperature was stable at 80 °C. TiO₂ (1 g) was added and the slurry was stirred at 80 °C. After 4 h, the stirring was stopped and the solution allowed to cool to room temperature. The solid was isolated via vacuum filtration and washed thoroughly with H₂O followed by ~ 100 mL 0.1 M NH₄OH, and then H₂O until the filtrate was pH 7 and absent of Au (NaBH₄ test, typically requires only a single 250 mL rinse) and Cl⁻ (AgNO₃ test, typically used another 500-750 mL). The washed solid was dried at room temperature under vacuum for 16 h. The catalysts were prepared by heating the supported precursors in flowing H₂ at 200 °C for 1 h. The catalysts were stored in the foil-wrapped vials at 4 °C under air.

General Catalytic Reaction Conditions

Reactions were performed in a 5 mL Kimax glass reactor with a Teflon septum sealed cap. 3 mL of toluene containing a 1 mM internal standard (1,2, 4-trichlobenzene) and 10 mg of the catalyst were heated for 10 min in the oil bath (silicon oil, Fischer) until the temperature reached 60 °C. Preliminary studies showed that it took the reaction vessel 5-7 min to reach 60 °C. The temperature was monitored via a thermometer placed in the oil bath that was controlled by a feedback thermocouple probe. The oil bath temperature was set to 63 °C. To assure homogenous heating and mixing, the oil bath was equipped with a stir bar and stirring was set to 900 RPM. Oxygen was allowed to flow through the headspace during the heating of the reaction and through the entirety of the reaction time. The flow of oxygen (2-5 sccm) was controlled by a mass flow controller. The desired amount of the substrate was added to the reaction vial to start the reaction. At desired times after the start of the reaction, 50 µL of the samples were taken using a

23G 1 mL syringe and was added to 3 mL of CH₂Cl₂ in an ice bath. 1 mL of this sample was filtered with 30 MM syringe filters into GC-MS vials. In a separate vial, 3 mL of toluene containing a 1 mM internal standard (1,2, 4-trichlobenzene) and the desired amount of the substrate were mixed to create a time zero sample. 50 μL of the solution in the vial was sampled for a data point at time zero. The sample was diluted in 3 mL of CH₂Cl₂. These samples were analyzed using GC-MS.

Gas Chromatography Mass Spectrometry (GC/MS)

Samples were analyzed using an Agilent 7820A GC System with a 7693-series auto injector and a 5977E network mass selective detector with a HP-5MS 5% phenyl methyl siloxane capillary column (dimensions 30 m x 250 µm x 0.25 µm). Carrier gas was UHP He, with1.2 mL/min flow rate. The oven temperature method consisted of a 3 min hold at 45 °C, followed by a ramp at 10 °C/min until it reached 150 °C. The ramp rate was then increased to 50 °C/min until it reached 250 °C. The method had a total run time of 15.5 min. Mass spectra were recorded after 3 min solvent delay. Peak areas were extracted manually.

Characterization details

Conventional and high-resolution TEM/STEM was performed at Columbia University Nanoinitiative (CNI) electron microscopy facilities using a FEI Talos F200X transmission/scanning transmission microscope. To prepare samples for TEM analysis, the solids were mixed with a minimal amount of 2-propanal and dropped onto a lacey carbon film on a Cu grid or a silicon nitride membrane grid with a membrane thickness of 50 nm, frame thickness of 50 µm and nine 0.1 mm x 0.1 mm windows and allowed to dry before collecting images. The operating voltage of the FEI Talos was 200 kV.

Particle Size Analysis

Using the STEM images for each catalyst, particle size analysis was performed using ImageJ. Software was calibrated using the scale bar at the bottom of each TEM image. Each particle was then individually measured, and the value was recorded. In total, 200 gold nanoparticles were measured for each catalyst to determine the average gold nanoparticle size and standard deviation for the distribution.

Elemental Analysis

Samples were sent to Galbraith labs to determine the mass % Au and F in the samples. CI-ODOL contained 1.3 mass percent Au and 0.53 mass percent F. For F-ODOL, the sample was 1.6 mass percent Au and 3.8 mass percent F.

Acknowledgements

The authors gratefully acknowledge the National Science Foundation (Grant CHE-1565843 to BF and RNA) for supporting this work.

Supporting information: Additional spectra, catalytic data, and more information on particle size analyses

References

- 1. Min, B. K.; Friend, C. M., Heterogeneous Gold-Based Catalysis for Green Chemistry: Low-Temperature CO Oxidation and Propene Oxidation. *Chem. Rev.* **2007**, *107* (6), 2709-2724.
- 2. Hughes, M. D.; Xu, Y.-J.; Jenkins, P.; McMorn, P.; Landon, P.; Enache, D. I.; Carley, A. F.; Attard, G. A.; Hutchings, G. J.; King, F.; Stitt, E. H.; Johnston, P.; Griffin, K.; Kiely, C. J., Tunable gold catalysts for selective hydrocarbon oxidation under mild conditions. *Nature* **2005**, *437* (7062), 1132-1135.
- 3. Biella, S.; Prati, L.; Rossi, M., Selective Oxidation of D-Glucose on Gold Catalyst. *J. Catal.* **2002**, *206* (2), 242-247.
- 4. Biella, S.; Prati, L.; Rossi, M., Selectivity control in the oxidation of phenylethane-1,2-diol with gold catalyst. *Inorganica Chimica Acta* **2003**, *349*, 253-257.
- 5. Carrettin, S.; McMorn, P.; Johnston, P.; Griffin, K.; Kiely, C. J.; Hutchings, G. J., Oxidation of glycerol using supported Pt, Pd and Au catalysts. *Phys Chem Chem Phys* **2003**, *5* (6), 1329-1336.

- 6. Wittstock, A.; Zielasek, V.; Biener, J.; Friend, C. M.; Bäumer, M., Nanoporous Gold Catalysts for Selective Gas-Phase Oxidative Coupling of Methanol at Low Temperature. *Science* **2010**, *327* (5963), 319-322.
- 7. Augugliaro, V.; Bellardita, M.; Loddo, V.; Palmisano, G.; Palmisano, L.; Yurdakal, S., Overview on oxidation mechanisms of organic compounds by TiO₂ in heterogeneous photocatalysis. *Journal of Photochemistry and Photobiology C: Photochemistry Reviews* **2012**, *13* (3), 224-245.
- 8. Fernández-García, M.; Wang, X.; Belver, C.; Hanson, J. C.; Rodriguez, J. A., Anatase-TiO₂ Nanomaterials: Morphological/Size Dependence of the Crystallization and Phase Behavior Phenomena. *The Journal of Physical Chemistry C* **2007**, *111* (2), 674-682.
- 9. Parker, S. C.; Campbell, C. T., Reactivity and sintering kinetics of Au/TiO₂(110) model catalysts: particle size effects. *Topics in Catalysis* **2007**, *44* (1), 3-13.
- 10. Liu, G.; Yang, H. G.; Pan, J.; Yang, Y. Q.; Lu, G. Q.; Cheng, H.-M., Titanium Dioxide Crystals with Tailored Facets. *Chemical Reviews* **2014**, *114* (19), 9559-9612.
- 11. Yang, H. G.; Sun, C. H.; Qiao, S. Z.; Zou, J.; Liu, G.; Smith, S. C.; Cheng, H. M.; Lu, G. Q., Anatase TiO_2 single crystals with a large percentage of reactive facets. *Nature* **2008**, *453* (7195), 638-641.
- 12. Fang, W. Q.; Gong, X.-Q.; Yang, H. G., On the Unusual Properties of Anatase TiO₂ Exposed by Highly Reactive Facets. *The Journal of Physical Chemistry Letters* **2011**, *2* (7), 725-734.
- 13. Cho, C. H.; Han, M. H.; Kim, D. H.; Kim, D. K., Morphology evolution of anatase TiO₂ nanocrystals under a hydrothermal condition (pH=9.5) and their ultra-high photo-catalytic activity. *Materials Chemistry and Physics* **2005**, *92* (1), 104-111.
- 14. Bennett, D. A.; Cargnello, M.; Diroll, B. T.; Murray, C. B.; Vohs, J. M., Shape-dependence of the thermal and photochemical reactions of methanol on nanocrystalline anatase TiO₂. *Surface Science* **2016**, *654*, 1-7.
- 15. Ye, L.; Mao, J.; Liu, J.; Jiang, Z.; Peng, T.; Zan, L., Synthesis of anatase TiO_2 nanocrystals with {101}, {001} or {010} single facets of 90% level exposure and liquid-phase photocatalytic reduction and oxidation activity orders. *J. Mater. Chem. A*, **2013**, *1*, 10532-10537.
- 16. Chen, S.; Zhang, B.; Su, D.; Huang, W., Titania Morphology-Dependent Gold–Titania Interaction, Structure, and Catalytic Performance of Gold/Titania Catalysts. *ChemCatChem* **2015**, *7* (20), 3290-3298.
- 17. Kim, S. S.; Lee, H. H.; Hong, S. C., The effect of the morphological characteristics of TiO₂ supports on the reverse water—gas shift reaction over Pt/TiO₂ catalysts. *Appl Catal B Environ.* **2012**, *119-120*, 100-108.
- 18. Yu, Z.; Zhang, Z.; Zhang, Y.; Huang, W., Titania Morphology-Dependent Catalysis of CuOx/TiO₂ Catalysts in CO Oxidation and Water Gas Shift Reactions. *ChemCatChem* **2020**, *12* (14), 3679-3686.
- 19. Li, D.; You, R.; Yang, M.; Liu, Y.; Qian, K.; Chen, S.; Cao, T.; Zhang, Z.; Tian, J.; Huang, W., Morphology-Dependent Evolutions of Sizes, Structures, and Catalytic Activity of Au Nanoparticles on Anatase TiO₂ Nanocrystals. *J. Phys. Chem. C* **2019**, *123* (16), 10367-10376.
- 20. Li, D.; Chen, S.; You, R.; Liu, Y.; Yang, M.; Cao, T.; Qian, K.; Zhang, Z.; Tian, J.; Huang, W., Titania-morphology-dependent dual-perimeter-sites catalysis by Au/TiO₂ catalysts in low-temperature CO oxidation. *J. Catal.* **2018**, *368*, 163-171.

- 21. Mahdavi-Shakib, A.; Sempel, J.; Babb, L.; Oza, A.; Hoffman, M.; Whittaker, T. N.; Chandler, B. D.; Austin, R. N., Combining Benzyl Alcohol Oxidation Saturation Kinetics and Hammett Studies as Mechanistic Tools for Examining Supported Metal Catalysts. *ACS Catal* **2020**, *10*, 10207-10215.
- 22. Kumar, G.; Tibbitts, L.; Newell, J.; Panthi, B.; Mukhopadhyay, A.; Rioux, R. M.; Pursell, C. J.; Janik, M.; Chandler, B. D., Evaluating differences in the active-site electronics of supported Au nanoparticle catalysts using Hammett and DFT studies. *Nature Chemistry* **2018**, *10*, 268-274.
- 23. Abad, A.; Corma, A.; García, H., Catalyst Parameters Determining Activity and Selectivity of Supported Gold Nanoparticles for the Aerobic Oxidation of Alcohols: The Molecular Reaction Mechanism. *Chemistry A European Journal* **2008**, *14* (1), 212-222.
- 24. Personick, M. L.; Madix, R. J.; Friend, C. M., Selective Oxygen-Assisted Reactions of Alcohols and Amines Catalyzed by Metallic Gold: Paradigms for the Design of Catalytic Processes. *ACS Catal.* **2017**, *7*, 965-985.
- 25. Fristrup, P.; Johansen, L. B.; Christensen, C. H., Mechanistic Investigation of the Gold-catalyzed Aerobic Oxidation of Alcohols. *Catal Lett* **2008**, *120*, 184-190.
- 26. Savara, A.; Chan-Thaw, C. E.; Sutton, J. E.; Wang, D.; Prati, L.; Villa, A., Molecular Origin of the Selectivity Differences between Palladium and Gold–Palladium in Benzyl Alcohol Oxidation: Different Oxygen Adsorption Properties. *ChemCatChem* **2017**, *9*, 253-257.
- 27. Hammett, L. P., The Effect of Structure upon the Reactions of Organic Compounds. Benzene Derivatives. *J. Am. Chem. Soc.* **1937**, *59* (1), 96-103.
- 28. Fristrup, P.; Tursky, M.; Madsen, R., Mechanistic investigation of the iridium-catalysed alkylation of amines with alcohols. *Org. Biomol. Chem.* **2012**, *10*, 2569-2577.
- 29. Mueller, J. A.; Goller, C. P.; Sigman, M. S., Elucidating the Significance of β-Hydride Elimination and the Dynamic Role of Acid/Base Chemistry in a Palladium-Catalyzed Aerobic Oxidation of Alcohols. *J. Am. Chem. Soc.* **2004**, *126*, 9724-9734.
- 30. Dijksman, A.; Marino-González, A.; Mairata i Payeras, A.; Arends, I. W. C. E.; Sheldon, R. A., Efficient and Selective Aerobic Oxidation of Alcohols into Aldehydes and Ketones Using Ruthenium/TEMPO as the Catalytic System. *J. Am. Chem. Soc.* **2001**, *123*, 6826-6833.
- 31. Thorson, M. K.; Klinkel, K. L.; Wang, J.; Williams, T. J., Mechanism of Hydride Abstraction by Cyclopentadienone-Ligated Carbonylmetal Complexes (M = Ru, Fe). *Eur. J. Inorg. Chem.* **2009**, 2009, 295-302.
- 32. Samuelsen, Simone V.; Santilli, C.; Ahlquist, M. S. G.; Madsen, R., Development and mechanistic investigation of the manganese(III) salen-catalyzed dehydrogenation of alcohols. *Chem Sci* **2019**, *10*, 1150-1157.
- 33. Mueller, J. A.; Jensen, D. R.; Sigman, M. S., Dual Role of (–)-Sparteine in the Palladium-Catalyzed Aerobic Oxidative Kinetic Resolution of Secondary Alcohols. *J. Am. Chem. Soc.* **2002**, *124*, 8202-8203.
- 34. Pirrung, M. C.; Morehead, A. T., Saturation Kinetics in Dirhodium(II) Carboxylate-Catalyzed Decompositions of Diazo Compounds. *J. Am. Chem. Soc.* **1996**, *118*, 8162-8163.
- 35. Collier, V. E.; Ellebracht, N. C.; Lindy, G. I.; Moschetta, E. G.; Jones, C. W., Kinetic and Mechanistic Examination of Acid—Base Bifunctional Aminosilica Catalysts in Aldol and Nitroaldol Condensations. *ACS Catal* **2016**, *6*, 460-468.

- 36. Wisser, F. M.; Berruyer, P.; Cardenas, L.; Mohr, Y.; Quadrelli, E. A.; Lesage, A.; Farrusseng, D.; Canivet, J., Hammett Parameter in Microporous Solids as Macroligands for Heterogenized Photocatalysts. *ACS Catal.* **2018**, *8*, 1653-1661.
- 37. Finiels, A.; Geneste, P.; Moreau, C., Transfer of concepts from homogeneous to heterogeneous catalysis: use of Hammett relationships to assess reaction mechanisms and nature of active sites in reactions catalyzed by sulfides, metals, clays and zeolites. *J. Mol. Catal. A: Chem.* **1996**, *107*, 385-391.
- 38. Hui, Y.; Zhang, S.; Wang, W., Recent Progress in Catalytic Oxidative Transformations of Alcohols by Supported Gold Nanoparticles. *Advanced Synthesis & Catalysis* **2019**, *361* (10), 2215-2235.
- 39. Wisser, F. M.; Berruyer, P.; Cardenas, L.; Mohr, Y.; Quadrelli, E. A.; Lesage, A.; Farrusseng, D.; Canivet, J., Hammett Parameter in Microporous Solids as Macroligands for Heterogenized Photocatalysts. *ACS Catal.* **2018**, *8* (3), 1653-1661.
- 40. Ro, I.; Resasco, J.; Christopher, P., Approaches for Understanding and Controlling Interfacial Effects in Oxide-Supported Metal Catalysts. *ACS Catalysis* **2018**, *8* (8), 7368-7387.
- 41. van Deelen, T. W.; Hernández Mejía, C.; de Jong, K. P., Control of metal-support interactions in heterogeneous catalysts to enhance activity and selectivity. *Nature Catalysis* **2019**, *2* (11), 955-970.
- 42. Cirri, A.; Hernández, H. M.; Johnson, C. J., High Precision Electronic Spectroscopy of Ligand-Protected Gold Nanoclusters: Effects of Composition, Environment, and Ligand Chemistry. *The Journal of Physical Chemistry A* **2020**, *124* (8), 1467-1479.
- 43. Cirri, A.; Morales Hernández, H.; Kmiotek, C.; Johnson, C. J., Systematically Tuning the Electronic Structure of Gold Nanoclusters through Ligand Derivatization. *Angewandte Chemie International Edition* **2019**, *58* (39), 13818-13822.
- 44. Cirri, A.; Silakov, A.; Jensen, L.; Lear, B. J., Probing ligand-induced modulation of metallic states in small gold nanoparticles using conduction electron spin resonance. *Physical Chemistry Chemical Physics* **2016**, *18* (36), 25443-25451.
- 45. Choudhary, V. R.; Dumbre, D. K., Supported Nano-Gold Catalysts for Epoxidation of Styrene and Oxidation of Benzyl Alcohol to Benzaldehyde. *Top. Catal.* **2009**, *52*, 1677-1687.
- 46. Choudhary, V. R.; Dumbre, D. K.; Bhargava, S. K., Oxidation of Benzyl Alcohol to Benzaldehyde by tert-Butyl Hydroperoxide over Nanogold Supported on TiO2 and other Transition and Rare-Earth Metal Oxides. *Industrial & Engineering Chemistry Research* **2009**, *48* (21), 9471-9478.
- 47. Enache, D. I.; Knight, D. W.; Hutchings, G. J., Solvent-free Oxidation of Primary Alcohols to Aldehydes using Supported Gold Catalysts. *Catalysis Letters* **2005**, *103* (1), 43-52.
- 48. Li, Y.; Shen, W., Morphology-dependent nanocatalysts: Rod-shaped oxides. *Chem. Soc. Rev.* **2014**, *43*, 1543-1574.
- 49. Susman, M. D.; Feldman, Y.; Vaskevich, A.; Rubinstein, I., Chemical Deposition of Cu₂O Nanocrystals with Precise Morphology Control. *ACS Nano* **2014**, *8* (1), 162-174.
- 50. Kuo, C.-H.; Hua, T.-E.; Huang, M. H., Au Nanocrystal-Directed Growth of Au–Cu₂O Core–Shell Heterostructures with Precise Morphological Control. *J. Am. Chem. Soc.* **2009**, *131* (49), 17871-17878.
- 51. Li, Y.; Liu, Q.; Shen, W., Morphology-dependent nanocatalysis: metal particles. *Dalton trans.* **2011**, *40*, 5811-5826.

- 52. Gordon, T. R.; Cargnello, M.; Paik, T.; Mangolini, F.; Weber, R. T.; Fornasiero, P.; Murray, C. B., Nonaqueous Synthesis of TiO₂ Nanocrystals Using TiF₄ to Engineer Morphology, Oxygen Vacancy Concentration, and Photocatalytic Activity. *J Am Chem Soc* **2012**, *134*, 6751-6761.
- 53. Panayotov, D. A.; Burrows, S. P.; Morris, J. R., Infrared Spectroscopic Studies of Conduction Band and Trapped Electrons in UV-Photoexcited, H-Atom n-Doped, and Thermally Reduced TiO₂. *J. Phys. Chem C.* **2012**, *116* (7), 4535-4544.
- 54. Mahdavi-Shakib, A.; Rahmani-Chokanlu, A.; Schwartz, T. J.; Austin, R. N.; Frederick, B. G., Implications of Electron Scavanging Character of Sulfated Titania for Photochemistry. *(in prep)* **2021**.
- 55. Panayotov, D.; Ivanova, E.; Mihaylov, M.; Chakarova, K.; Spassov, T.; Hadjiivanov, K., Hydrogen spillover on Rh/TiO₂: the FTIR study of donated electrons, co-adsorbed CO and H/D exchange. *Phys Chem Chem Phys* **2015**, *17* (32), 20563-73.
- 56. Panayotov, D. A.; Yates, J. T., n-Type doping of TiO_2 with atomic hydrogen-observation of the production of conduction band electrons by infrared spectroscopy. *Chemical Physics Letters* **2007**, *436* (1), 204-208.
- 57. Minella, M.; Faga, M. G.; Maurino, V.; Minero, C.; Pelizzetti, E.; Coluccia, S.; Martra, G., Effect of Fluorination on the Surface Properties of Titania P25 Powder: An FTIR Study. *Langmuir* **2010**, *26* (4), 2521-2527.
- 58. Selloni, A., Anatase shows its reactive side. *Nature Materials* **2008,** *7* (8), 613-615.
- 59. Mino, L.; Pellegrino, F.; Rades, S.; Radnik, J.; Hodoroaba, V.-D.; Spoto, G.; Maurino, V.; Martra, G., Beyond Shape Engineering of TiO₂ Nanoparticles: Post-Synthesis Treatment Dependence of Surface Hydration, Hydroxylation, Lewis Acidity and Photocatalytic Activity of TiO₂ Anatase Nanoparticles with Dominant {001} or {101} Facets. *ACS Applied Nano Materials* **2018**, *1* (9), 5355-5365.
- 60. Mahdavi-Shakib, A.; Arce-Ramos, J. M.; Austin, R. N.; Schwartz, T. J.; Grabow, L. C.; Frederick, B. G., Frequencies and Thermal Stability of Isolated Surface Hydroxyls on Pyrogenic TiO₂ Nanoparticles. *The Journal of Physical Chemistry C* **2019**, *123* (40), 24533-24548.
- 61. Sheng, H.; Zhang, H.; Song, W.; Ji, H.; Ma, W.; Chen, C.; Zhao, J., Activation of Water in Titanium Dioxide Photocatalysis by Formation of Surface Hydrogen Bonds: An In Situ IR Spectroscopy Study. *Angewandte Chemie International Edition* **2015**, *54* (20), 5905-5909.
- 62. Di Valentin, C.; Pacchioni, G.; Selloni, A., Reduced and n-Type Doped TiO₂: Nature of Ti3+ Species. *The Journal of Physical Chemistry C* **2009**, *113* (48), 20543-20552.
- 63. Peng, Y.-K.; Chou, H.-L.; Edman Tsang, S. C., Differentiating surface titanium chemical states of anatase TiO₂ functionalized with various groups. *Chemical Science* **2018**, *9* (9), 2493-2500.
- 64. Zanella, R.; Giorgio, S.; Henry, C. R.; Louis, C., Alternative Methods for the Preparation of Gold Nanoparticles Supported on TiO₂. *J. Phys. Chem B* **2002**, *106*, 7634-7642.
- 65. Ivanova, S.; Pitchon, V.; Petit, C., Application of the direct exchange method in the preparation of gold catalysts supported on different oxide materials. *Journal of Molecular Catalysis A: Chemical* **2006**, *256* (1), 278-283.
- 66. Gong, X.-Q.; Selloni, A.; Dulub, O.; Jacobson, P.; Diebold, U., Small Au and Pt Clusters at the Anatase $TiO_2(101)$ Surface: Behavior at Terraces, Steps, and Surface Oxygen Vacancies. *J. Am. Chem. Soc.* **2008**, *130* (1), 370-381.

- 67. Han, Y.; Liu, C.-j.; Ge, Q., Interaction of Pt Clusters with the Anatase TiO2(101) Surface: A First Principles Study. *The Journal of Physical Chemistry B* **2006**, *110* (14), 7463-7472.
- 68. Pellegrino, F.; Sordello, F.; Mino, L.; Minero, C.; Hodoroaba, V.-D.; Martra, G.; Maurino, V., Formic Acid Photoreforming for Hydrogen Production on Shape-Controlled Anatase TiO₂ Nanoparticles: Assessment of the Role of Fluorides, {101}/{001} Surfaces Ratio, and Platinization. *ACS Catalysis* **2019**, *9* (8), 6692-6697.
- 69. Xiong, Z.; Lei, Z.; Chen, X.; Gong, B.; Zhao, Y.; Zhang, J.; Zheng, C.; Wu, J. C. S., CO₂ photocatalytic reduction over Pt deposited TiO₂ nanocrystals with coexposed {101} and {001} facets: Effect of deposition method and Pt precursors. *Catalysis Communications* **2017**, *96*, 1-5.
- 70. Conte, M.; Miyamura, H.; Kobayashi, S.; Chechik, V., Spin Trapping of Au–H Intermediate in the Alcohol Oxidation by Supported and Unsupported Gold Catalysts. *J. Am. Chem. Soc.* **2009**, *131*, 7189-7196.
- 71. Fujitani, T.; Nakamura, I.; Takahashi, A., H2O Dissociation at the Perimeter Interface between Gold Nanoparticles and TiO2 Is Crucial for Oxidation of CO. *ACS Catalysis* **2020**, *10* (4), 2517-2521.
- 72. Fujitani, T.; Nakamura, I.; Akita, T.; Okumura, M.; Haruta, M., Hydrogen Dissociation by Gold Clusters. *Angew Chem Int Ed Engl* **2009**, *48*, 9515-9518.
- 73. Fujitani, T.; Nakamura, I., Mechanism and Active Sites of the Oxidation of CO over Au/TiO2. *Angewandte Chemie International Edition* **2011**, *50* (43), 10144-10147.
- 74. Panthi, B.; Mukhopadhyay, A.; Tibbitts, L.; Saavedra, J.; Pursell, C. J.; Rioux, R. M.; Chandler, B. D., Using Thiol Adsorption on Supported Au Nanoparticle Catalysts To Evaluate Au Dispersion and the Number of Active Sites for Benzyl Alcohol Oxidation. *ACS Catalysis* **2015**, *5* (4), 2232-2241.
- 75. Banerjee, S.; Zangiabadi, A.; Mahdavi-Shakib, A.; Husremovic, S.; Frederick, B. G.; Barmak, K.; Austin, R. N.; Billinge, S. J. L., Quantitative Structural Characterization of Catalytically Active TiO2 Nanoparticles. *ACS Applied Nano Materials* **2019**, *2* (10), 6268-6276.
- 76. Wang, H.; Lu, J., A Review on Particle Size Effect in Metal-Catalyzed Heterogeneous Reactions. *Chinese Journal of Chemistry* **2020**, *38* (11), 1422-1444.
- 77. Janssens, T. V. W.; Carlsson, A.; Puig-Molina, A.; Clausen, B. S., Relation between nanoscale Au particle structure and activity for CO oxidation on supported gold catalysts. *Journal of Catalysis* **2006**, *240* (2), 108-113.
- 78. van Bokhoven, J. A.; Miller, J. T., d Electron Density and Reactivity of the d Band as a Function of Particle Size in Supported Gold Catalysts. *The Journal of Physical Chemistry C* **2007**, 111 (26), 9245-9249.
- 79. Haruta, M.; Tsubota, S.; Kobayashi, T.; Kageyama, H.; Genet, M. J.; Delmon, B., Low-Temperature Oxidation of CO over Gold Supported on TiO2, α -Fe2O3, and Co3O4. *Journal of Catalysis* **1993**, *144* (1), 175-192.
- 80. Yao, Q.; Wang, C.; Wang, H.; Yan, H.; Lu, J., Revisiting the Au Particle Size Effect on TiO2-Coated Au/TiO2 Catalysts in CO Oxidation Reaction. *The Journal of Physical Chemistry C* **2016**, *120* (17), 9174-9183.
- 81. Cargnello, M.; Doan-Nguyen, V. V. T.; Gordon, T. R.; Diaz, R. E.; Stach, E. A.; Gorte, R. J.; Fornasiero, P.; Murray, C. B., Control of Metal Nanocrystal Size Reveals Metal-Support Interface Role for Ceria Catalysts. *Science* **2013**, *341* (6147), 771.

- 82. Hervier, A.; Baker, L. R.; Komvopoulos, K.; Somorjai, G. A., Titanium Oxide/Platinum Catalysis: Charge Transfer from a Titanium Oxide Support Controls Activity and Selectivity in Methanol Oxidation on Platinum. *The Journal of Physical Chemistry C* **2011**, *115* (46), 22960-22964.
- 83. Lin, F.; Chen, Y.; Zhang, L.; Mei, D.; Kovarik, L.; Sudduth, B.; Wang, H.; Gao, F.; Wang, Y., Single-Facet Dominant Anatase TiO₂ (101) and (001) Model Catalysts to Elucidate the Active Sites for Alkanol Dehydration. *ACS Catalysis* **2020**, *10* (7), 4268-4279.
- 84. Caps, V.; Arrii, S.; Morfin, F.; Bergeret, G.; Rousset, J.-L., Structures and associated catalytic properties of wel-defined nanoparticles produced by laser vaporisation of alloy rods. *Faraday Discuss* **2008**, *138*, 241-256.
- 85. Dhaene, E.; Billet, J.; Bennett, E.; Van Driessche, I.; De Roo, J., The Trouble with ODE: Polymerization during Nanocrystal Synthesis. *Nano Letters* **2019**, *19* (10), 7411-7417.
- 86. Zanella, R.; Giorgio, S.; Henry, C. R.; Louis, C., Alternative Methods for the Preparation of Gold Nanoparticles Supported on TiO₂. *J. Phys. Chem B* **2002**, *106* (31), 7634-7642.
- 87. Ivanova, S.; Pitchon, V.; Petit, C., Application of the direct exchange method in the preparation of gold catalysts supported on different oxide materials. *J. Mol. Catal. A: Chem.* **2006**, *256*, 278-283.